Journal of The Electrochemical Society, **159** (2) D124-D128 (2012)
0013-4651/2012/159(2)/D124/5/$28.00 © The Electrochemical Society

An Alternative Method to Grow Ge Thin Films on Si by Electrochemical Deposition for Photonic Applications

M. J. Jawad,[a] M. R. Hashim,[a] N. K. Ali,[b,z] E. P. Córcoles,[c] and Maneea E. Sharifabad[b]

[a]*School of Physics, Universiti Sains Malaysia, 11800-Penang, Malaysia,*
[b]*Material Innovations and Nanoelectronics Research Group, Faculty of Electrical Engineering, Ibnu Sina Institute for Fundamental Science Studies, and* [c]*Faculty of Biomedical and Health Science Engineering Universiti Teknologi Malaysia, 81310 Skudai, Johor, Malaysia*

Germanium films several micrometers in thickness were electrochemically deposited on silicon wafers for the first time without catalysts and at room temperature from a solution containing Ge species that have been electrochemically dissolved from Ge target. The films were investigated using scanning electron microscopy (SEM), X-ray diffraction (XRD), and Raman spectroscopy. SEM images show that the deposited products presented different structures (Flower-like, spheres, and thin films) depending on the current density. XRD reveals that the germanium electrodeposits were of polycrystalline structure and have the preferred crystallographic growth orientation of (220). The grown films were deposited with nickel contact electrodes for characterization as Metal semiconductor Metal (MSM) photodiodes. The current-voltage (I-V) measurements showed the ability to efficiently detect both UV and visible photons. The low deposition temperature, the ease of thickness control, and the inherent advantage of spatial selectivity of the electrodeposition process make this method a promising way to selectively grow high-quality germanium for electronic device applications.
© 2011 The Electrochemical Society. [DOI: 10.1149/2.090202jes] All rights reserved.

Manuscript submitted August 23, 2011; revised manuscript received November 15, 2011. Published December 22, 2011.

In seeking new materials, researchers have focused on substitutes with superior electronic properties to complement and eventually replace Si.[1,2] Indeed, Ge has regained some popularity in the field of semiconductor electronics due to its high mobility and thus providing an alternative to Si for high performance devices.[3] Currently, light detection in the UV spectral range technology utilizes wide-bandgap materials. These include metal zinc oxide and magnesium zinc oxide, III-V materials as well as Schottky-type TiO UV photodiodes. These materials are grown on incompatible substances. Si and Ge-based optical photodiodes are sensitive to visible and infrared radiation; their responsivity in the UV region is low in its bulk structure since the room temperature bandgap energy of Si is only 1.2 eV and 0.65 eV for Ge. Contrary to bulk Si, Si nanoparticles exhibit behavior of direct wide-bandgap materials. This makes it very sensitive to UV light and transparent to visible light. Nayfeh et al.[4] presented UV photodetectors with superior efficiency created by deposition of Si nanoparticle films on Si substrates. Ge has smaller electron and hole effective masses and a larger dielectric constant than Si, the effective Bohr radius of the excitons in Ge ($\sim$25.3 nm) is larger than that in Si (4 nm). This implies that the quantum confinement effects for Ge nanoparticles can be seen at a much larger size,[5] hence showing a larger shift of an optical band gap (blue shift) than the Si nanoparticles. So far, to the best of our knowledge, there is no report about utilizing elemental Ge nanoparticles for UV/visible detection.

Germanium based thin films have been prepared mainly using a variety of physical and chemical methods. Among popular physical methods are RF-sputtering,[6] evaporation-condensation,[7] chemical vapor deposition,[8] and electron beam evaporation.[9] While these techniques provide nanocrystal Ge and thin films, they all present some difficulties besides high operating costs. Alternatively, cost effective chemical solution methods have been widely used for the preparation of freestanding colloid nanocrystals.[10,11] However, it is still a challenge to synthesize Si and Ge nanocrystals using chemical methods, mainly due to their strong covalent bonding and the need for high temperature and pressure to promote crystallization.[12]

Electrochemical deposition is an inexpensive and fast synthesis of semiconductor thin films and nanostructures.[13] There were few reported studies in the last decade about germanium.[14–16] Endres et al.[17–19] recently reported a nanoscale electrodeposition of Ge and Si from ionic liquids. In this work we report for the first time the fabrication of a new UV/visible photodetector using Ge-processing that utilizes the new Ge nanoparticle material. Germanium nanocrystals were prepared by electrochemical etching of Ge target followed by electrochemical deposition of these Ge species on Si substrate. This was followed by the fabrication of MSM Ni/Ge/Si photodetectors. Surface morphology and crystal structure of the deposited Ge films were investigated using scanning electron microscopy (SEM), X-ray diffraction and Raman spectroscopy. I-V characteristics of the fabricated photodetectors will also be discussed.

Experimental

Our method consists of two steps; firstly, the preparation of solution contains Ge species by electrochemical etching of the Ge target, secondly, the electrochemical deposition of the Ge species on Si substrate to produce Ge thin films. A piece of Ge (99.999% pure, 30 mm $\times$ 10 mm $\times$ 5 mm) was immersed in a Teflon Beaker containing an electrolyte mixture of HF (49%):Ethanol (95%), 1:4. The Ge target was connected to the anode and a Pt wire immersed in the electrolyte acted as a cathode. A current density of 300 mA/cm^2 (electropolishing regime) was applied for 3 hours. The substrates used for the deposition of the Ge thin films were n-type silicon wafers with (100) orientation and resistivity of 1–10 Ω cm. Prior to the deposition, the 2” Si wafer was cut into 4 pieces and cleaned using RCA cleaning method. The Si piece was pressed to a Teflon cell at an open window fit to quarter 2” Si wafer. Between the Si piece and the bottom of the cell an *O* ring was used to seal the cell. The Si piece was connected to the cathode and a Pt wire was immersed in the solution as an anode. The solution was obtained during the first step (etching step). Samples were prepared using different current densities (7.5 for samples (a) and (b) and 5 and 2.5 mA/cm^2 for samples (c) and (d), respectively) for one hour at room temperature. After deposition, the samples were washed several times with deionized water and dried in ambient air. The structural properties of the samples were investigated using scanning electron microscopy (SEM), X-ray diffraction and Raman spectrometer (equipped with an argon ion (Ar^+) laser with $\lambda = 514$ nm).

Ni/Ge/Si MSM photodiodes were then fabricated. Prior to the deposition of contact electrodes, samples were dipped in acetone and methanol to clean the surface. A 300 nm thick Ni film was subsequently deposited onto the sample surface by DC sputtering to serve as metal contacts. Metal masks were used to define the interdigitated contact pattern. The fingers of the Ni contact electrodes were 230 μm wide and 3.5 mm long with 400 μm spacing. The active area of the whole device was 4×4 mm^2. Photocurrent and dark current of the

[z] E-mail: nihad@fke.utm.my

fabricated photodiodes were then measured by using Keithley source measure unit (model No. 2400).

Results and Discussion

Chemical analysis and surface morphology.— Germanium is not appreciably affected by water and resists concentrated hydrochloric acid, sulfuric acid, hydrofluoric acid and sodium hydroxide solutions, even at their boiling points.[20] The material is quite stable in air up to 400°C where slow oxidation begins and becomes noticeably more rapid above 600°C. Germanium is attacked by electrochemical anodization. However, high current densities are necessary, since germanium reacts slowly at low current densities. Due to the wetting properties of ethanol, Ge presents higher solubility in ethanol than in water. Hydrogen bubbles produced during the electrochemical etching of Ge in aqueous solutions form a passivation layer on the Ge surface, impairing solubility processes. Surface passivation is reduced in ethanol, accounting for the higher solubility observed in these electrolytes.[21]

Electrochemical etching of germanium in aqueous HF solution (anodic regime) does not apparently present germanium oxides. In hydrofluoric acid, quadrivalent germanium forms hydrogen hexafluorogermanate, a six-coordinated complex;[22]

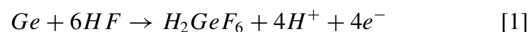

$$Ge + 6HF \rightarrow H_2GeF_6 + 4H^+ + 4e^- \quad [1]$$

Hydrogen hexafluorogermanate in water dissociates, hence upon anodization the electrolyte solution is rich in hexafluorogermanate ions.

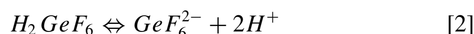

$$H_2GeF_6 \Leftrightarrow GeF_6^{2-} + 2H^+ \quad [2]$$

Exposure of the freshly prepared surface to ambient conditions leads to oxidation. The hydrolysis of hexafluorogermanates in water is autocatalytic and takes place by a solvolytic dissociation mechanism.

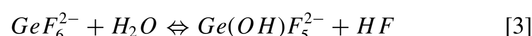

$$GeF_6^{2-} + H_2O \Leftrightarrow Ge(OH)F_5^{2-} + HF \quad [3]$$

This reaction is followed by rapid hydrolysis of the $Ge(OH)F_5{}^{2-}$ ion to GeO_2.[22] Ge surfaces have been previously investigated by constantly changing the polarization direction and the cathodic reactions were observed to proceed in two steps: 1) GeO_2 species at the surface are reduced, 2) hydrogen atoms are binding to Ge surface. Germanium hydride compounds are then formed at the surface of the cathode[23]

$$Ge + 4e^- + 4H^+ \rightarrow GeH_4 \quad [4]$$

Liang et al.[24] investigations of the cathodic electrodeposition of Ge on Au(111) in aqueous solutions showed the formation of two well-ordered hydroxide phases upon initial reduction of the Ge(IV) species. Further reduction resulted in germanium hydride structures, in a two-electron process mechanism. Electrodeposition of Ge from $GeCl_4$ in ionic liquids showed two reduction peaks in the cyclovoltammograms, indicating the reduction of Ge(IV) to Ge (II) and this to Ge crystals.[19] Hence, we suggest the electrodeposition of Ge from hexafluorogermanate ions in the electrolyte to occur via two reduction processes, from oxidation state IV to II and finally to germanium metal (oxidation state zero).

In this study, the electrodeposition of germanium thin films was carried out at constant current densities. Under these conditions, the potential alters its value accordingly, to maintain the current constant. The potential shifts when the concentration of electroactive species at the electrode surface drops to zero, assuming that the kinetics of the electrode reaction does not limit the current. Upon the reduction process of Ge (IV) to Ge (0), the material is deposited on the surface of the cathode (silicon wafer) as shown in Fig. 1.

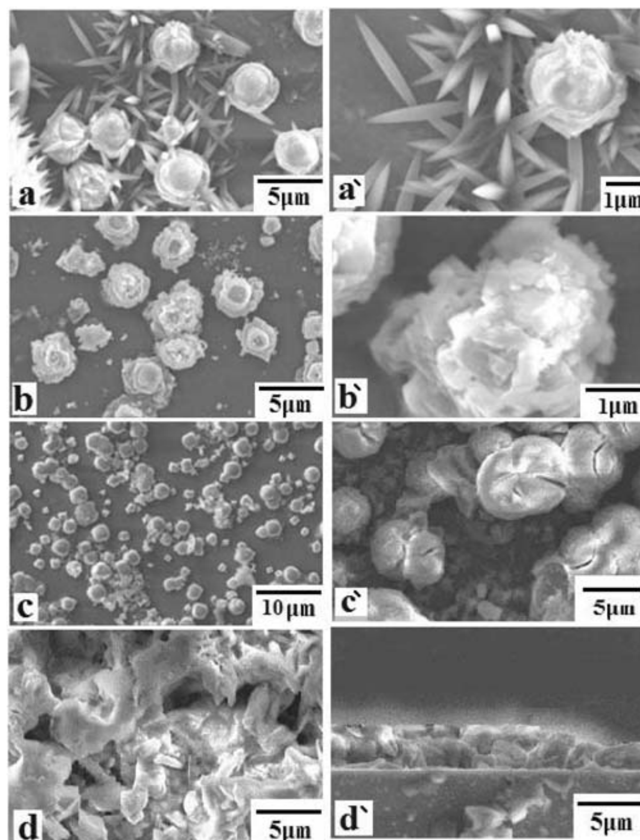

Figure 1. SEM images of samples (a) to (d). Samples are electrochemically deposited Ge thin films on Si at different current densities; (a) 7.5 mA/cm^2, (b) 7.5 mA/cm^2 (copper eliminated), c) 5 mA/cm^2, and d) 2.5 mA/cm^2. Image d') shows the cross section of sample (d).

Figures 1a and 1a′ illustrate SEM images of our first attempt to deposit crystalline Ge on Si with current density of 7.5 mA/cm^2. Flower-like structures, with diameters of 3 μm and distributed with an average distance from each other of 5 μm approximately, were observed. Interestingly, between these flower-like structures, a grass-like pattern was also observed as can be appreciated on the close up image at higher magnification in Fig. 1a′. EDX measurements of these Ge deposits were conducted in order to examine further these structures. While the flower-like structures were confirmed to be pure Ge, EDX measurements (not shown here) revealed the composition of the grass-like structures to be copper. The existence of copper is due to the migration of copper ions from the copper wire, which is connected to the Ge target during the etching process.[25] Diffusing metal atoms is characteristic of metals at very high current density. The acceptor property of Cu in Ge and the high diffusivity of Cu suggest that 1) both substitutional (Cu_s) and interstitial (Cu_i) copper atoms exist and 2) there is a strong dependence of Cu diffusion on the structural perfection of the Ge crystal.[26] In order to prevent migration of copper, undesirable for electronic devices, a Pt wire was connected between the piece of Ge metal and the anode of the power supply. In this case, the grass-like pattern structures were eliminated producing only pure Ge flower-like structures (without grass) as shown in Fig. 1b and 1b′.

The growth mechanism of these flower-like structures is not understood yet. The lattice mismatch between Ge and Si is ∼4.17%. This fact motivated the early attempts to grow high quality Ge nucleation sites on Si substrates. Due to the lattice mismatch between Ge and Si, a wet Ge layer was grown first, and once the critical thickness was obtained, the strain was released and Ge nucleation sites were formed. However, we hypothesize that the flower-like structures are not the

result of this growth mechanism, but rather that Ge ions, attracted by the Si substrate, are deposited as droplets onto the surface of Si as soon as the current begins to flow. These micro-sized Ge nucleation sites may act as microelectrodes, where the current flow might experience a greater rate and lower resistance than in the case of Si substrate. Ge presents higher mobility than Si and the Ge particles layered on the Si surface would have accumulated a charge density. Hence, the Ge ions will be attracted by these nucleation sites, forming layers of Ge deposits and increasing in size to create Ge spherical crystals of $\sim$3 μm diameter illustrated in Fig. 1 samples (a) and (b). As experimentally observed, these closed spherical structures open into flower-like structures probably due to release of gases during the growth process and/or during the drying process. In order to grow uniform layers of Ge, lower current density was applied. Fig. 1c and 1c′ show a Ge film deposited on Si surface at 5 mA/cm^2. The Ge crystals produced in this case are not uniform, presenting cracks on the surface.

Lastly, a uniform Ge layer of $\sim$3 μm thickness was obtained using a current density of 2.5 mA/cm^2 as shown in Fig. 1d. The deposited germanium has a defined spherical morphology in Fig. 1c with a diameter larger than 5 μm. In contrast, Fig. 1d shows compact and uniform deposits. Fig. 1d′ illustrates the cross section of sample (d), $\sim$3 μm Ge layer obtained at 2.5 mA/cm^2 for one hour deposition time. The current efficiency of the Ge deposition at 2.5 mA/cm^2 was therefore approximately 94%, confirming the superiority of this current density. This number disagrees with previous studies on Ge electrodeposition from non aqueous[27] and aqueous solutions.[24] In a recent publication, Chandrasekharan et al.[28] reported current efficiency of 51% during anodic depositions at 3 mA/cm^2 and claimed this to be the result of the limited side reactions at the anode. The quantity of Ge deposited and the morphology of the voltammograms are strongly influenced by the pH of the solution, being the highest Ge depositions in aqueous solutions at pH 9.32.[24] This suggests that the acid character of our solution might reduce the reactions at the cathode. However, with 1 hour deposition times, Ge is deposited in a slow and uniform rate, while side reactions are eliminated.

Experiments were repeated with current density of 1 and 3.5 mA/cm^2 for samples (e) and (f), respectively. SEM images of these Ge structures revealed compact needle-type morphologies (Fig. 2), which differ from those shown in Fig. 1. A possible explanation might be the different quantities of H_2O and O_2. Huang et al.[29] reported that a considerable amount of water, adsorbed from air in an aged solution, resulted in anisotropic structures. The increase of water or oxygen levels in the bath solution over time, might produce a layer of germanium oxides. In fact, samples a, b and c, unlike sample d, showed traces of GeO_2 in the Raman spectra (Fig. 4). Higher amount of GeO_2 could be the cause of the different morphologies in samples (e) and (f). Although exact mechanisms of Ge growth using this technique are still very much to be explored, these results confirm the feasibility of the Ge films growth on Si with this method.

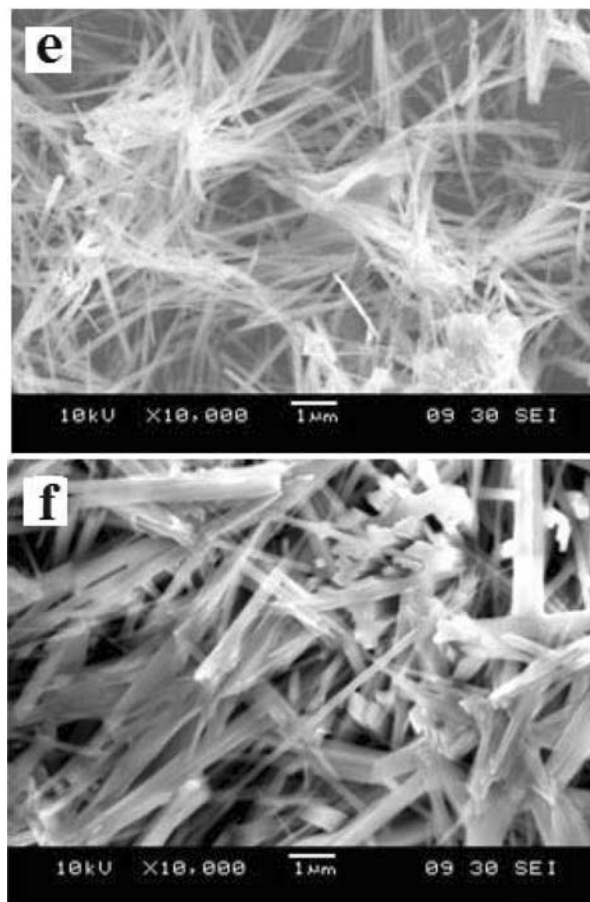

Figure 2. SEM images of samples (e) and (f). Image (e) and (f) refer to the samples of electrodeposited Ge films prepared using current density of 1 and 3.5 mA/cm^2, respectively.

X Ray diffraction.— Crystallographic orientation of the germanium thin films grown on the Si (100) were determined using the X-ray diffraction (XRD) for samples (a), (b), (c), and (d) (Fig. 3). All samples present sharp peaks at $2\theta = 33$ and 69.2°, which are associated with the diffraction from the (200) and (400) planes of Si substrate, respectively. The spectrum of sample (a) shows two peaks associated to (111) and (220) Ge plane. Furthermore, two additional peaks at $2\theta = 43$ and 50 degree, associated to (111) and (200) planes, respectively, illustrate the existence of Cu in the sample.[30] The peaks related to Cu were not present in the X-ray diffraction patterns of samples (b), (c), and (d). Sample (c) shows only one peak, associated to (220) Ge plane, while the peak associated to (111) Ge plane is observed again in sample (d) with an additional peak at (400) Ge plane. These results show that the deposited Ge nanostructures were of poly crystalline and having the preferred crystallographic growth orientation of (220).

Raman spectra.— Figure 4 shows the Raman spectra of the deposited Ge samples (a, b, c, and d) and the spectrum of c-Ge for comparison. The spectrum of c-Ge was obtained from the Ge target used to prepare the solution and it shows the fundamental Raman line at 300 cm^{-1}. Samples (a), (b), and (c) present a strong peak at

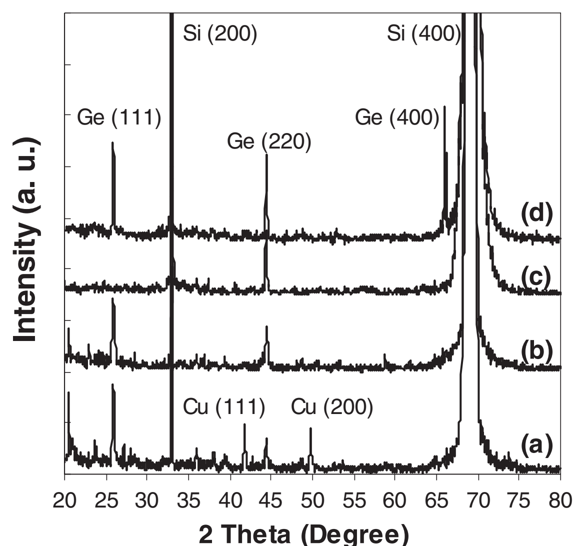

Figure 3. X-ray diffraction (XRD) pattern of the electrodeposited Ge samples (a, b, c, and d) illustrating the preferred crystallographic orientation of the germanium thin films grown on Si.

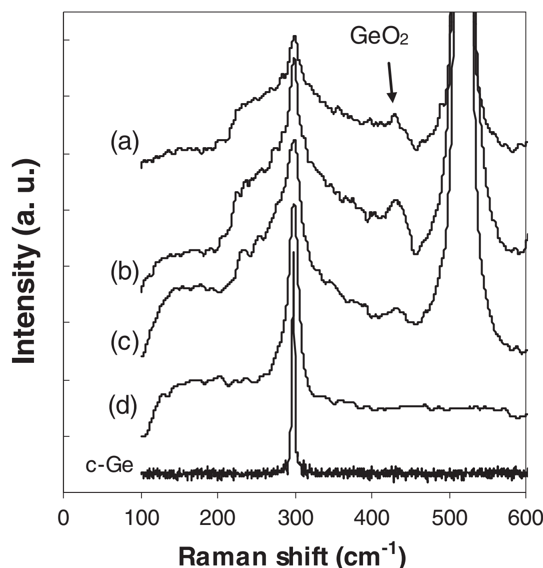

Figure 4. Raman spectra of the electrodeposited Ge samples (a, b, c, and d) and the spectrum of c-Ge for comparison. The spectrum of c-Ge shows the fundamental Raman line at 300 cm^{-1}. Si phonon mode peak at 520 cm^{-1} is present only in samples (1a, 1b, and 1c).

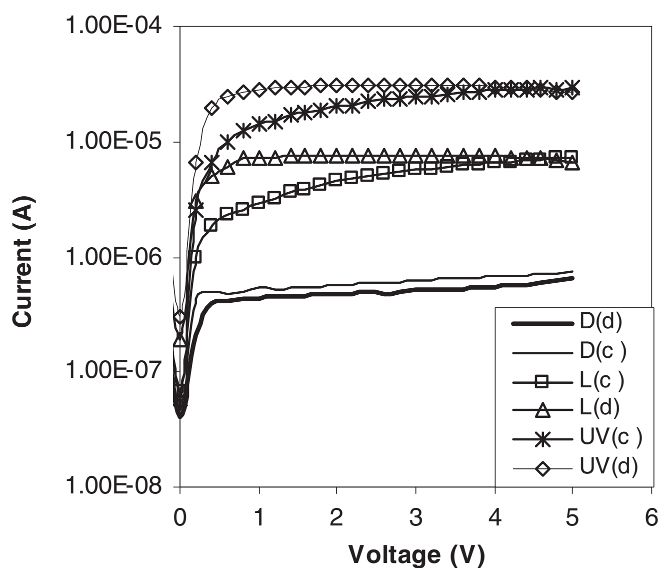

Figure 5. Measured current-voltage characteristics of the Ni/Ge/Si MSM photodetectors using samples (c) and (d) under dark (D), incandescent light (L), and UV light (UV) conditions.

520 cm^{-1} that corresponds to the Si phonon mode from the Si substrate. However, this peak is not present in sample (d) due to the thicker, uniform Ge layer deposited on the Si substrate. The Raman spectrum of sample (a), shows a broad peak at 300 cm^{-1}, indicating amorphous Ge phonon band.[31] We observed a hump on the left-hand side of the peak, which developed into small peaks located at 273 and 241 cm^{-1} on the spectra of samples (b) and (c), probably due to Ge_{III}.[32] Bundy and Jasper[33] reported that Ge_{III} transformed completely to Ge_I (cubic Ge) in 6 h when heated to 200°C. The Ge-Ge peak (∼300 cm^{-1}) developed into a sharper shape in the subsequent samples, indicating good crystalline Ge layer. Furthermore, an additional peak at ∼430 cm^{-1} can be observed in samples (a, b, and c), which indicates the presence of GeO_2 traces and hence confirms that these deposited Ge structures are not pure Ge.[34] The spectrum of sample (d), deposited at low current density (2.5 mA/cm^2), on the other hand illustrates a sharp peak at 300 cm^{-1} and the absence of the peak associated to GeO_2 (430 cm^{-1}). This proves that this sample was a single crystalline structure and more importantly, free of any GeO_2 traces.

Figure 5 shows the room-temperature I–V characteristics of the Ni/Ge/Si MSM photodetectors fabricated with samples (c) and (d). This was measured using Keithley source measure unit (model No. 2400) in the dark, under illumination of incandescent white light, and UV light. It can be seen that the samples showed a very good response to photons. It is not surprising that these samples are sensitive to incandescent white light and UV light since their photoluminescence spectra (data not shown here) has two peaks, a sharp peak located at 400 nm and a broad peak located at 500 nm. With a 5 V applied bias, it was found that the leakage current of samples (c) and (d) were 7.37×10^{-7} A and 6.36×10^{-7} A, respectively. The dark current is due to leakage from imperfections and cracks in the film. It can be seen that both dark current and photocurrent increase rapidly with voltage when the applied voltage is small. However, these currents start to saturate at about 0.5 V for sample (d), while for sample (c) the current continues to increase with voltage up to 5 V and then saturates with the same value as for sample (d). These results suggest that the currents were probably related to generation-recombination centers and were limited by carrier lifetime (η). Results also indicate that sample (d) presents higher photocurrent to dark-current contrast ratio (gain). Thus, higher detection sensitivity in both incandescent and the UV regions are found, due to the smaller dark current of sample (d) compared with sample (c). We obtained gains up to 65 for UV light and 27 for incandesccent light for sample (d) at 1 V, while for sample (c) it was 16 and 6 for UV light and incandescent light, respectively. This is due to sample quality and uniformity as indicated from Raman spectra of these samples (Fig. 4). We can see that the spectrum of sample (c) is broader than that of sample (d) and have a hump on left side indicating the existance of amorphous Ge layer and non-uniform size structures. The gain is related to the size uniformity of the nanocrystalline films. Size uniformity provides uniform confinement energies and bandgaps (3.1 eV). Uniform bandgaps allow resonant tunneling between particles, which is much faster than nonresonant processes. Resonant tunneling-limited transport provides higher carrier mobility, hence shorter transit time (t) according to $t = d^{2/\mu V}$ (assuming a single electron-hole mobility), where V is the applied bias, d is the film thickness, and μ is the effective mobility.[4]

Conclusions

Ge films were electrochemically deposited by a simple cost effective technique. Results show that the uniformity of the films deposited on the Si substrate is dependent on the current density. The sample deposited at low current density (2.5 mA/cm^2) was more uniform than samples deposited at higher current densities (5–7.5 mA/cm^2). The XRD patterns show that the Ge electrodeposited films are of crystalline structure and have the preferred crystallographic growth orientation (220). Raman spectra for all four samples show a line corresponding to cubic Ge (300 cm^{-1}) related to the scattering of Ge–Ge, where current density of 2.5 mA/cm^2 produced higher crystallite quality. Ni/Ge/Si MSM UV/visible photodetectors were also fabricated. The device showed a good response to both visible and UV light producing the current gains at 1V of 27 and 65, respectively. This method showed that it is possible to grow high quality Ge layers using a low cost technique for photonic applications.

References

1. X. L. Wua, G. G. Siu, Y. Gu, N. Tang, T. Gao, and X. M. Bao, *Appl. Phys. Lett.*, **74**, 827 (1999).
2. R. K. Roy and A. K. Pal, *Materials Letters*, **59**, 2204 (2005).
3. M. S. Song, J. H. Jung, Y. Kim, Y. Wang, J. Zou, H. J. Joyce, Q. Gao, H. H. Tan, and C. Jagadish, *Nanotechnology*, **19**, 125602 (2008).
4. O. M. Nayfeh, S. Rao, A. Smith, J. Therrien, and M. H. Nayfeh, *IEEE Photonics Technology Letters*, **16**, 1927 (2004).

5. Y. Maeda, N. Tsuamoto, Y. Yazawa, Y. Kanemitsu, and Y. Masumoto, *Appl. Phys. Lett.*, **64**, 3168 (1991).
6. S. K. Ray and K. Das, *Opt. Mater*, **27**, 948 (2005).
7. A. Stella, P. Tognini, C. E. Bottani, P. Milani, P. Cheyssac, and R. Kofman, *Thin Solid Films*, **318**, 100 (1998).
8. Z. He, J. Xu, W. Li, K. Chen, and D. Feng, *J. Non-Cryst. Solids*, **266–269**, 1025 (2000).
9. Q. Wan, C. L. Lin, W. L. Liu, and T. H. Wang, *Appl. Phys. Lett.*, **82**, 4708 (2003).
10. H. Miguez, V. Fornes, F. Meseguer, F. Marquez, and C. Lopez, *Appl. Phys. Lett.*, **69**, 2347 (1996).
11. J. P. Carpenter, C. M. Lukehart, D. O. Henderson, R. Mu, B. D. Jones, R. Glosser, S. R. Stock, J. E. Wittig, and J. G. Zhu, *Chem. Mater.*, **8**, 1268 (1996).
12. W. Z. Wang, J. Y. Huang, and Z. F. Ren, *Langmuir*, **21**, 751 (2005).
13. D. Lincot, *Thin Solid Films*, **487**, 40 (2005).
14. S. M. Gates, D. D. Koleske, J. R. Heath, and M. Copel, *Appl. Phys. Lett.*, **62**, 510 (1993).
15. C. D. Lokhande and S. H. Pawar, *Phys. Stat. Sol.*, **111**, 17 (1989).
16. F. Endres and S. Z. El Abedin, *Phys. Chem. Chem. Phys.*, **4**, 1640 (2002).
17. S. Zein El Abedin, N. Borissenko, and F. Endres, *Electrochemistry Communications*, **6**, 510 (2004).
18. S. Zein El Abedin, E. M. Moustafa, R. Hempelmann, H. Natter, and F. Endres, *ChemPhysChem*, **7**, 1535 (2006).
19. R. Al-Salman, S. Zein El Abedin, and F. Endres, *Phys. Chem. Chem. Phys.*, **10**, 4650 (2008).
20. O. H. Johnson, *Chem. Rev.*, **51**, 431 (1952).
21. E. Rojas, B. Terheiden, J. Hensen, W. Köstler, W. Zimmermann, G. Strobl, H. Plagwitz, and R. Brendel, *the European Photovoltaic Solar Energy Conference*, Hamburg, Germany, Sept. (2009).
22. V. A. Nazarenko and A. M. Andrianov, *Russ. Chem. Rev.*, **34**, 547 (1965).
23. D. Turner, *J. Electrochem. Soc.*, **103**, 252 (1956).
24. X. Liang, Y-G. Kim, D. K. Gebergziabiher, and J. L. Stickney, *Langmuir*, **26**, 2877 (2010).
25. L. Y. Wei, *Journal of Physics and Chemistry of Solids*, **18**, 162 (1961).
26. N. A Stolwijk, W. Frank, J. Holzl, S. J. Pearton, and E. E Haller, *Journal of Applied Physics*, **57**, 5211 (1985).
27. Q. Huang, S. W. Bedell, K. L. Saenger, M. Copel, H. Deligianni, and L. T. Romankiwa, *Electrochemical and Solid-State Letters*, **10**, D124-D126 (2007).
28. N. Chandrasekharan and S. C. Sevov, *Journal of The Electrochemical Society*, **157**, C140-C145 (2010).
29. Q. Huang, H. Deligianni, and L. T. Romankiw, *Electrochemical and Solid-State Letters*, **10**, D121-D123 (2007).
30. K. S. Kim, H. C. Jeong, J. Y. Cho, D. H. Kang, H. K. Kim, H. M. Yoo, and I. W. Shim, *Bull. Korean Chem. Soc.*, **24**, 647 (2003).
31. Y. Sasaki and C. Horie, *Phys Rev B*, **47**, 3811 (1993).
32. R. Alben, J. E. Smith, and D. Weaire, *Phys. Rev. Lett.*, **30**, 1141 (1973).
33. F. P. Bundy and J. S. Jasper, *Science*, **139**, 340 (1963).
34. M. J. Jawad, M. R. Hashim, and N. K. Ali, *Electrochemical and Solid-State Letters*, **14**, D17 (2011).